



Advances in thermoelectric $(\text{GeTe})_x(\text{AgSbTe}_2)_{100-x}$

Hongxia Liu(刘虹霞), Xinyue Zhang(张馨月), Wen Li(李文), and Yanzhong Pei(裴艳中)

Citation: Chin. Phys. B, 2022, 31 (4): 047401. DOI: 10.1088/1674-1056/ac3cae

Journal homepage: <http://cpb.iphy.ac.cn>; <http://iopscience.iop.org/cpb>

What follows is a list of articles you may be interested in

Two-dimensional square- Au_2S monolayer: A promising thermoelectric material with ultralow lattice thermal conductivity and high power factor

Wei Zhang(张伟), Xiao-Qiang Zhang(张晓强), Lei Liu(刘蕾), Zhao-Qi Wang(王朝棋), and Zhi-Guo Li(李治国)

Chin. Phys. B, 2021, 30 (7): 077405. DOI: 10.1088/1674-1056/abe115

Thermal stability and thermoelectric properties of Cd-doped nano-layered Cu_2Se prepared using NaCl flux method

Jianhua Lu(陆建华), Decong Li(李德聪), Wenting Liu(刘文婷), Lanxian Shen(申兰先), Jiali Chen(陈家莉), Wen Ge(葛文), and Shukang Deng(邓书康)

Chin. Phys. B, 2020, 29 (12): 127403. DOI: 10.1088/1674-1056/abbbf5

Electrical and thermoelectric study of two-dimensional crystal of NbSe_2

Xin-Qi Li(李新祺), Zhi-Lin Li(李治林), Jia-Ji Zhao(赵嘉佳), Xiao-Song Wu(吴孝松)

Chin. Phys. B, 2020, 29 (8): 087402. DOI: 10.1088/1674-1056/ab9614

Synthesis, physical properties, and annealing investigation of new layered Bi-chalcogenide LaOBiHgS_3

Yi Yu(于一), Chunchang Wang(汪春昌), Liang Li(李亮), Qiuju Li(李秋菊), Chao Cheng(程超), Shuting Wang(王舒婷), Changjin Zhang(张昌锦)

Chin. Phys. B, 2019, 28 (1): 017401. DOI: 10.1088/1674-1056/28/1/017401

Directional mechanical and thermal properties of single-layer black phosphorus by classical molecular dynamics

Afira Maryam, Ghulam Abbas, Muhammad Rashid, Atif Sattar

Chin. Phys. B, 2018, 27 (1): 017401. DOI: 10.1088/1674-1056/27/1/017401

Advances in thermoelectric $(\text{GeTe})_x(\text{AgSbTe}_2)_{100-x}$

Hongxia Liu(刘虹霞)^{1,2}, Xinyue Zhang(张馨月)³, Wen Li(李文)^{3,†}, and Yanzhong Pei(裴艳中)^{3,‡}

¹School of Materials Science and Engineering, Taiyuan University of Science and Technology, Taiyuan 030024, China

²Laboratory of Magnetic and Electric Functional Materials and the Applications, The Key Laboratory of Shanxi Province, Taiyuan 030024, China

³Interdisciplinary Materials Research Center, School of Materials Science and Engineering, Tongji University, Shanghai 201804, China

(Received 11 October 2021; revised manuscript received 16 November 2021; accepted manuscript online 24 November 2021)

The $(\text{GeTe})_x(\text{AgSbTe}_2)_{100-x}$ alloys, also called TAGS- x in short, have long been demonstrated as a promising candidate for thermoelectric applications with successful services as the p-type leg in radioisotope thermoelectric generators for space missions. This largely stems from the complex band structure for a superior electronic performance and strong anharmonicity for a low lattice thermal conductivity. Utilization of the proven strategies including carrier concentration optimization, band and defects engineering, an extraordinary thermoelectric figure of merit, zT , has been achieved in TAGS-based alloys. Here, crystal structure, band structure, microstructure, synthesis techniques and thermoelectric transport properties of TAGS-based alloys, as well as successful strategies for manipulating the thermoelectric performance, are surveyed with opportunities for further advancements. These strategies involved are believed to be in principle applicable for advancing many other thermoelectrics.

Keywords: thermoelectric, TAGS, band structure, lattice thermal conductivity, thermoelectric figure of merit

PACS: 74.25.fg, 74.25.fc, 74.25.F–, 81.20.–n

DOI: 10.1088/1674-1056/ac3cae

1. Introduction

Thermoelectric technology, which enables a mutual conversion between heat and electricity through carrier transport within a solid, has been widely used in power generation and refrigeration without moving parts, emissions and noise. The conversion efficiency is dominantly determined by the thermoelectric materials' dimensionless figure of merit, $zT = S^2T/\rho(\kappa_E + \kappa_L)$, where S , T , ρ , κ_E , and κ_L are the Seebeck coefficient, absolute temperature, electrical resistivity, and electronic and lattice components of thermal conductivity, respectively. Thus, a highly efficient thermoelectric material requires a high S , a low ρ , but a low κ . However, the electronic parameters including S , ρ , and κ_E are strongly coupled with each other through the carrier concentration, leading it difficult to obtain a net increase in zT by optimizing one single parameter.

The κ_L is the only independent parameter determining the thermoelectric performance. Therefore, κ_L -minimization becomes a mainstream to enhance the thermoelectric performance of materials. This can be effectively realized by introducing various defects, such as zero-dimensional point defects,^[1–6] one-dimensional dislocations^[7,8] and two-dimensional interfaces,^[9–12] for effectively scattering phonons and thereby reducing κ_L . Moreover, the features of complex crystal structure,^[13,14] liquid-like ions,^[15] low sound velocity,^[16] and strong lattice anharmonicity^[17,18] have been demonstrated to accompany with an intrinsic low κ_L , which

are utilized as guiding principles for exploring novel thermoelectric materials with a superior zT .

Due to the existence of amorphous low-boundary limit of κ_L for a given material, numerous efforts have been devoted to enhancing the electronic performance at optimal carrier concentrations. Band engineering, including band convergence^[19]/nestification^[20] for high band degeneracy (N_v), has been proposed and demonstrated to effectively decouple the correlation among the electronic parameters (S , ρ , and κ_E). This strategy enables a significant zT -enhancement in many thermoelectric materials, such as PbTe,^[19] SnTe,^[21,22] GeTe,^[23] CoSb₃,^[24] Mg₂Si,^[25] Zintl compounds^[26] and Te.^[20] Note that the small inertial effective mass (m_1^*)^[27] and low deformation potential coefficient (E_{def})^[28] are proven to be beneficial for the high electronic performance as well.

The $\text{IV}_A\text{--VI}_A$ semiconductors, typically PbTe,^[29,30] SnTe^[31,32] and GeTe^[33,34] in a cubic structure, have been widely demonstrated as promising p-type thermoelectric materials with an extraordinary zT . This largely comes from the coexistence of both L and Σ valence bands with a small energy offset (ΔE), where the L and Σ bands have a high band degeneracy (N_v) of 4 and 12, respectively.^[35] Therefore, a high effective N_v up to 16 can be achieved by aligning the L and Σ bands, leading to an enhancement in zT .

Recently, the crystal structure for rhombohedral GeTe has been revealed to be a directional distortion of the cubic one along $[111]$ with the interaxial angle reducing from 90° (cubic)

[†]Corresponding author. E-mail: liwen@tongji.edu.cn

[‡]Corresponding author. E-mail: yanzhong@tongji.edu.cn

to 88.2° (rhombohedral) at room temperature.^[23] Such a distortion leads to an opposite arrangement in energy of the L and Σ valence bands in rhombohedral GeTe, namely, low-energy L band and high-energy Σ band. This unique band structure guarantees a possibility of band manipulation and thereby a superior electronic performance in rhombohedral GeTe. Eventually, a peak zT higher than 2 has been achieved in rhombohedral GeTe with a further help of κ_L -reduction.^[23]

As a derivative of GeTe, $(\text{GeTe})_x(\text{AgSbTe}_2)_{100-x}$ alloys, also called “TAGS- x ” (tellurium-antimony-germanium-silver), have long been considered as a promising candidate for p-type thermoelectric applications due to the high $zT > 1.0$ in a broad temperature range. In fact, TAGS- x have been successfully utilized in radioisotope thermoelectric generators (RTG) for space missions. Numerous efforts have been devoted to zT -advancements of TAGS- x focusing on x within 75–90. TAGS alloys retain the major features of the band structure of GeTe, which inspires a band engineering by manipulating AgSbTe₂ concentration for zT -enhancement.^[36] Moreover, compositional optimization and doping for power factor improvement^[37,38] and microstructure engineering for κ_L -reduction^[39,40] have also been used for thermoelectric performance enhancements of TAGS alloys.

In this review, we summarize the characteristics of crystal structure, band structure and microstructure of TAGS alloys for understanding the origin of superior thermoelectric performance. The effective strategies leading to a great advancement in thermoelectric performance of TAGS are surveyed. The development of TAGS-based thermoelectric devices is also summarized.

2. Crystal structure of TAGS alloys

$(\text{GeTe})_x(\text{AgSbTe}_2)_{100-x}$ alloys can be regarded as quasi-binary solid solutions of GeTe and AgSbTe₂. At room temperature, AgSbTe₂ crystallizes in a rock-salt structure (space group of $Fm\bar{3}m$) in which Te occupies the anion site while Ag and Sb occupy the cation site randomly.^[41] GeTe exhibits a rock-salt structure ($Fm\bar{3}m$) only at $T > 720$ K, and undergoes a phase transition to a rhombohedral structure (space group of $R\bar{3}m$) at $T < 720$ K.^[42] TAGS alloys maintain the crystal structure features of GeTe, and the phase transition is also observed in TAGS- x alloys with $x \geq 80$.^[43,44] Figure 1 shows the crystal structure of $(\text{GeTe})_{85}(\text{AgSbTe}_2)_{15}$ (TAGS-85), as an example of TAGS- x . For high-temperature cubic phase of TAGS-85 ($Fm\bar{3}m$), Ge, Ag and Sb occupy the cation sites (1/2, 1/2, 1/2), and Te occupies the anion site (0, 0, 0).^[45]

The low-temperature rhombohedral phase with an asymmetric structure can be regarded as the result of the directional distortion of the cubic structure along [111].^[45] The breaking of the symmetry leads to a split of the diffraction peak into a doublet in the x-ray diffraction (XRD) pattern with decreasing temperature (Fig. 2(a)).^[46] This is further confirmed

by the change of the interaxial angle with decreasing temperature, suggesting a phase transition temperature of 510 K in TAGS-85 with an interaxial angle of 89.1° at room temperature (Fig. 2(b)).^[46] The interaxial angle for TAGS- x has been illustrated to increase with decreasing x , corresponding to an increase in phase transition temperature. In addition, the interaxial angle increases to 90° when $x < 80$, therefore, the TAGS alloys with $x < 80$ show a cubic structure at room temperature.^[36]

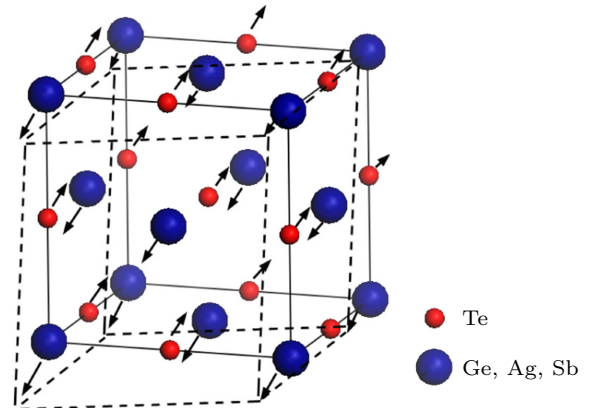


Fig. 1. Crystal structures of both cubic (solid line) and rhombohedral phases (dashed line) for TAGS. The arrows indicate the lattice distortion from cubic to rhombohedral.^[45] Reproduced under the terms of the CC-BY Creative Commons Attribution 3.0 License.^[45] Copyright 2014, IOP Publishing Ltd and Deutsche Physikalische Gesellschaft.

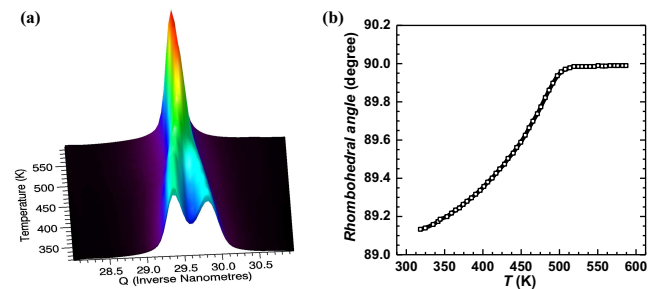


Fig. 2. Temperature dependent XRD patterns (a) and interaxial angle as a function of temperature (b) for TAGS-85 alloys.^[46] Reprinted from Ref. [46], with the permission of AIP Publishing. Copyright 2007 American Institute of Physics.

3. Band structure of TAGS alloys

The parameters of band structure, including the band degeneracy near Fermi level (N_v), band effective mass (m_b^*) and band gap (E_g), provide a detailed understanding of charge carrier transport properties. TAGS alloys retain not only the crystal structure but also the band structure of GeTe. Figure 3 shows the effect of rhombohedral distortion on the Brillouin zone and the hole Fermi surfaces in degenerately doped TAGS.^[45] The distortion splits $4L$ carrier pockets into $1T + 3L$ and 12Σ pockets into $6\eta + 6\Sigma$ in the Brillouin zone, respectively. Moreover, the $6\eta + 6\Sigma$ valence bands become the high-energy bands as well as valence band maximum in rhombohedral TAGS alloys. This opens many possibilities for increasing the overall N_v up to 16 by aligning the valence bands for enhanced electronic performance in TAGS alloys.

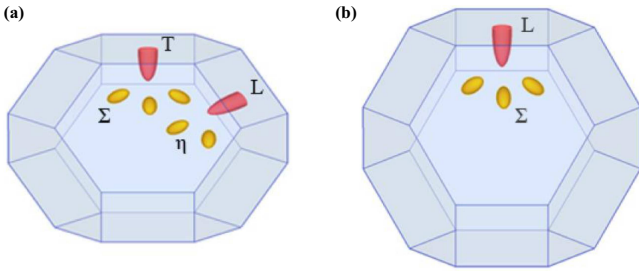


Fig. 3. The Brillouin zones and Fermi surfaces for rhombohedral (a) and cubic (b) phases of TAGS.^[45] Reproduced under the terms of the CC-BY Creative Commons Attribution 3.0 License.^[45] Copyright 2014, IOP Publishing Ltd and Deutsche Physikalische Gesellschaft.

The density of state (DOS) effective mass ($m_d^* = N_v^{2/3} m_b^*$) for the different valence bands is calculated assuming the m_b^* of $0.51 m_e$ for η and Σ bands and $1.15 m_e$ for L and T bands.^[45] The calculated results are listed in Table 1. The increased N_v enables multiple channels contributing to the charge transport and thus increases the electrical conductivity without explicitly decreasing the Seebeck coefficient. The m_d^* significantly increases with increasing N_v , enabling a superior electronic performance for rhombohedral TAGS alloys.

Table 1. Possible configurations of bands participating in transport and resulting degeneracy and calculated density of state effective mass (m_d^*).^[45] Reproduced under the terms of the CC-BY Creative Commons Attribution 3.0 License.^[45] Copyright 2014, IOP Publishing Ltd and Deutsche Physikalische Gesellschaft.

Pockets participating in conduction	Degeneracy N_v	Calculated m_d^*/m
$1 \times T$	1	1.15
$1 \times T, 3 \times L$	4	2.89
$1 \times T, 3 \times L, 6 \times \eta$	1	3.69
$1 \times T, 3 \times L, 6 \times \eta, 6 \times \Sigma$	16	4.42

4. Microstructure of TAGS alloys

The lattice thermal conductivity (κ_L) is an important parameter determining thermoelectric performance, and a low κ_L is essential for realizing extraordinary zT . TAGS alloys show a low κ_L , which is long considered to originate from the strong point defect phonon scattering by the alloying of GeTe and AgSbTe₂. Until 2000s, the presence of nanoscale compositional modulations is revealed to be responsible for the low κ_L in the PbTe-AgSbTe₂ (LAST) alloys,^[47] which promotes many researchers to focus on the microstructures of TAGS for understanding the origin of the low κ_L .

The *in-situ* elevated-temperature transmission electron microscopy (TEM) observation on TAGS-85 alloy shows the presence of twin-boundary defects (Fig. 4(a)) along with high-density antiphase domains (Fig. 4(b)) in rhombohedral TAGS.^[46,48] The twins are the result of inherently structural modulations, causing by the lattice strain imposed by the rhombohedral distortion along the [111] crystallographic direction. Moreover, nanodomains with a typical size of ~ 10 nm are found in the TAGS-80,^[49] as shown in Fig. 5. The large number of twin-boundary defects and nanodomains provide the extra sources for phonon scattering in TAGS alloys.

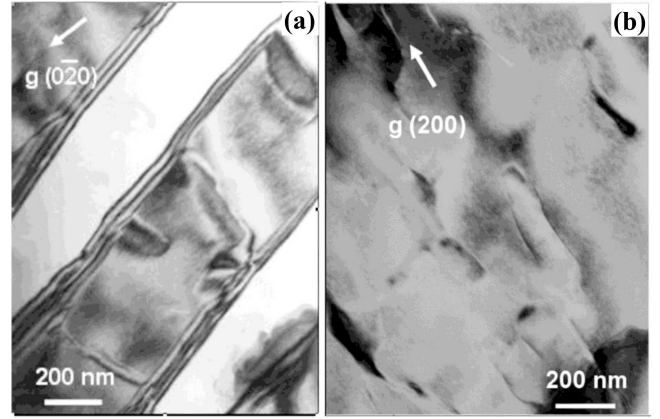


Fig. 4. Bright field TEM images of twinning (a) and antiphase domains (b) in as-solidified TAGS-85.^[46] Reprinted from Ref. [46], with the permission of AIP Publishing. Copyright 2007 American Institute of Physics.

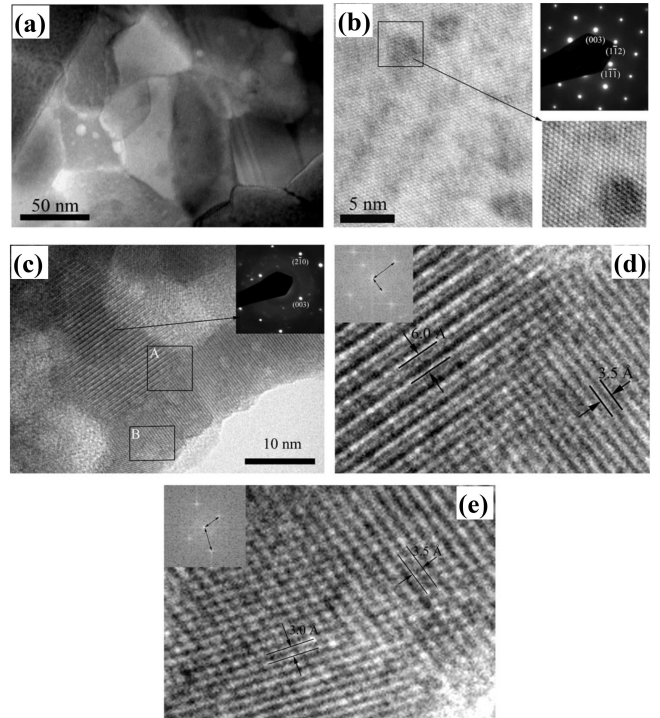


Fig. 5. Low-resolution TEM image (a) and high-resolution TEM image and selected area electron diffraction (SAED) pattern (b), (c) and magnified high magnification regions of A (d) and B (e) with the fast Fourier transforms (FFT).^[49] Republished with permission of IOP Publishing Ltd, from Ref. [49]; permission conveyed through Copyright Clearance Center, Inc. Copyright 2008 IOP Publishing Ltd.

Based on the TEM observations on TAGS-80 and TAGS-85 alloys, the microstructure features are found to be related to the composition. The atom probe tomography (APT) measurements are carried out on TAGS-50 and TAGS-85 alloys for clarifying the difference in microstructure.^[39] High-density Ag- and Sb-rich nanoprecipitates are observed in TAGS-50 alloy (Fig. 6(a)). However, TAGS-85 alloy shows an appearance of Ag- and Ge-rich precipitates (Fig. 6(b)). All these defects observed in the TAGS alloys with different compositions would contribute to the low lattice thermal conductivity.

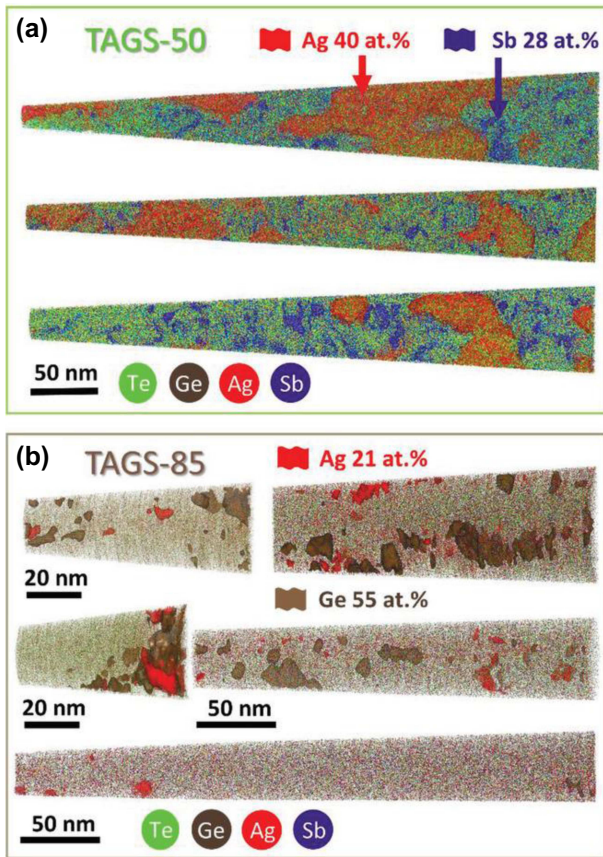


Fig. 6. The 3D APT maps of TAGS-50 (a) and TAGS-85 (b).^[39] Reproduced under the terms of the Creative Commons CC BY License.^[39] Copyright 2020 The Authors, published by Wiley-VCH Verlag GmbH & Co. KGaA, Weinheim.

5. Thermoelectric properties of TAGS alloys

5.1. Synthesis of TAGS alloys

The thermoelectric properties of TAGS- x alloys with different x have been widely investigated. GeTe-rich TAGS alloys ($x \geq 75$) are proven to have a high zT , which largely stems from the superior electronic performance. Thus, existing investigations in TAGS mostly focus on compositions of $x \geq 75$. Thermoelectric properties of TAGS- x alloys are highly sensitive to the synthesis process. Minor phases including Ge-rich and Ag-rich phases, or Ag_8GeTe_6 are frequently observed in TAGS alloys due to the high vapor pressures for the volatile elements of Te and Sb.^[48,50–52]

The techniques used to synthesize TAGS alloys could fall into three categories: (1) melting (M) and annealing (A) approach, which involves melting of pure elements with subsequent annealing and consolidating processes; (2) melt spinning (MS); (3) high-energy ball milling (BM). The latter two techniques are particularly applicable for preparing materials with fine grain, followed by a high-temperature sintering by hot-press (HP) or spark plasma sintering (SPS). The details of the synthesis techniques and relevant thermoelectric performance for the reported TAGS- x alloys with different x are listed in Table 2. It is found that quite different zT s can be realized in alloys with the same nominal composition. This

can be presumably understood by the different phase compositions and microstructures of the obtained samples using different synthesis methods, which determine the thermoelectric properties. The phase compositions of TAGS are highly related to the synthesis process, due to the greatly different vapor pressures for the constituent elements. Taking TAGS-85 for example, single-phase rhombohedral samples exhibit the best thermoelectric properties.^[50] The precipitation such as Ag_8GeTe_6 is detrimental to its electronic performance.^[50,53] However, the single-phase TAGS-85 can only be obtained by careful control of the synthesis conditions, such as annealing at an intermediate temperature for a long holding time, whereas shorter holding time gives multiphase mixtures of rhombohedral phases with slightly different lattice parameters, and even the metastable cubic phase, implying the variation of chemical compositions.^[53] Moreover, the distributions of microstructures mentioned above for TAGS are diverse with different synthesis methods,^[39,40,49,54–56] which involve the difference of homogeneity, grain size, crystallinity and the dimension of microstructures.

Table 2. Synthesis techniques and thermoelectric performance of the TAGS- x alloys.

Samples	Synthesis method	zT_{max}
TAGS-75 ^[57]	MA+HP	1.0/750 K
TAGS-75 ^[49]	M+HP	1.5/720 K
TAGS-75 ^[58]	M+SPS	0.7/625 K
TAGS-80 ^[57]	MA+HP	1.5/750 K
TAGS-80 ^[49]	M+HP	1.5/720 K
TAGS-80 ^[59]	MA+SPS	1.0/750 K
TAGS-80 ^[51]	M+HP	1.75/773 K
TAGS-85 ^[57]	MA+HP	1.4/750 K
TAGS-85 ^[38]	M	1.2/700 K
TAGS-85 ^[37]	M	1.3/730 K
TAGS-85 ^[49]	M+HP	1.5/720 K
TAGS-85 ^[59]	MA+SPS	1.4/700 K
TAGS-85 ^[51]	M+HP	1.4/773 K
TAGS-85 ^[50]	MA	1.3/773 K
TAGS-85 ^[53]	MA	0.4/673 K
TAGS-85 ^[60]	MA+SPS	1.4/727 K
TAGS-82, TAGS-87, TAGS-90 ^[59]	MA+SPS	0.8/750 K
TAGS-90 ^[57]	MA+HP	1.0/750 K
TAGS-90 ^[49]	M+HP	0.5/720 K
$(\text{GeTe})_{75}(\text{AgSbTe}_2)_{23.75}(\text{AgSbSe}_2)_{1.25}$ ^[58]	M+SPS	1.2/625 K
$(\text{GeTe})_{0.8}[(\text{Ag}_2\text{Te})_{0.4}(\text{Sb}_2\text{Te}_3)_{0.6}]_{0.2}$ ^[61]	MA	1.7/700 K
$(\text{Ge}_{0.96}\text{Sb}_{0.04}\text{Te})_{0.9}[(\text{Ag}_2\text{Te})_{0.4}(\text{Sb}_2\text{Te}_3)_{0.6}]_{0.1}$ ^[36]	MA+HP	1.8/725 K
$(\text{Ge}_{0.97}\text{Sb}_{0.03}\text{Te})_{0.8}[(\text{Ag}_2\text{Te})_{0.4}(\text{Sb}_2\text{Te}_3)_{0.6}]_{0.2}$ ^[36]	MA+HP	1.8/700 K
TAGS-85+1% Ce ^[38]	M	1.5/700 K
TAGS-85+1% Yb ^[38]	M	1.5/700 K
TAGS-85+1% Yb ^[54]	BM+HP	1.8/730 K
TAGS-85+1% Dy ^[37]	M	1.5/730 K
$\text{Ge}_{0.74}\text{Ag}_{0.13}\text{Sb}_{0.11}\text{Nd}_{0.02}\text{Te}$ ^[60]	MA+SPS	1.65/727 K
$(\text{Ag}_{0.8}\text{SbTe}_{1.9})_{15}(\text{GeTe})_{85}$ ^[62]	M+MS+HP	1.5/750 K
$(\text{Ag}_{0.8}\text{SbTe}_{1.9})_{15}(\text{GeTe})_{85}$ ^[62]	M+HP	1.4/750 K
$(\text{Ag}_{1.02}\text{Sb}_{0.98}\text{Te}_{1.98})_{15}(\text{GeTe})_{85}$ ^[63]	M+HP	1.4/744 K
$(\text{Ag}_{0.6}\text{SbTe}_{1.8})_{15}(\text{GeTe})_{85}$ ^[45]	M+HP	1.5/700 K
$(\text{Ag}_{0.6}\text{SbTe}_{1.8})_{15}(\text{GeTe})_{85}$ ^[40]	M+MS+HP	1.6/750 K
$\text{Ge}_{0.53}\text{Ag}_{0.13}\text{Sb}_{0.27}\square_{0.07}\text{Te}_1$ ^[64]	MA	1.3/433 K
$(\text{GeTe})_{90}(\text{Ag}_y\text{Sb}_{2-y}\text{Te}_{3-y})_{10}$ ^[65]	M+HP	1.7/770 K
$(\text{GeTe})_{5.5}\text{AgIn}_{0.5}\text{Sb}_{0.5}\text{Te}_2$ ^[66]	MA+HP	0.75/573 K

5.2. Ag/Sb ratio manipulation

The AgSbTe_2 can be regarded as a solid solution between Ag_2Te and Sb_2Te_3 . Thus, the TAGS- x alloys can be further expressed as $(\text{GeTe})_x[(\text{Ag}_2\text{Te})_{0.5}(\text{Sb}_2\text{Te}_3)_{0.5}]_{100-x}$, in which the tuning of Ag/Sb atomic ratio has been proven to be an efficient approach for enhancing thermoelectric performance of TAGS. The deviation of stoichiometry in AgSbTe_2 towards the Sb_2Te_3 side can lead to an obviously higher zT in TAGS-based alloys.^[40,45,61,65] Study of several compositions in the system $(\text{GeTe})_{1-x}[(\text{Ag}_2\text{Te})_{1-y}(\text{Sb}_2\text{Te}_3)_y]_x$ with $y = 0.6$ and $y = 0.75$ shows that the sample of $x = 0.2$, $y = 0.6$ has a high zT of 1.68 at 700 K.^[61] The peak zT of 1.7 has been realized in the TAGS-90 alloys with a Ag/Sb ratio of 2/3, which is 30% higher than that of $(\text{GeTe})_{90}(\text{AgSbTe}_2)_{10}$.^[65] Additionally, the manipulation of the Ag/Sb ratio is also used in $(\text{GeTe})_{85}(\text{Ag}_x\text{SbTe}_{x/2+1.5})_{15}$ with $x = 0.4-1.2$ for thermoelectric performance enhancement. It is found that the carrier concentration can be tuned in a broad range of $3 \times 10^{20}-12.5 \times 10^{20} \text{ cm}^{-2}$ (Fig. 7(a)) by manipulating the Ag/Sb ratio.^[45] Interestingly, an increased m_d^* is obtained in the samples with high carrier concentrations (Fig. 7(b)), which is stated to be attributed to the increased N_V by Fermi level deepening into the low-lying valence band. Thus, the increased m_d^* enables an increase in Seebeck coefficient as well as electronic performance (Fig. 7(c)).

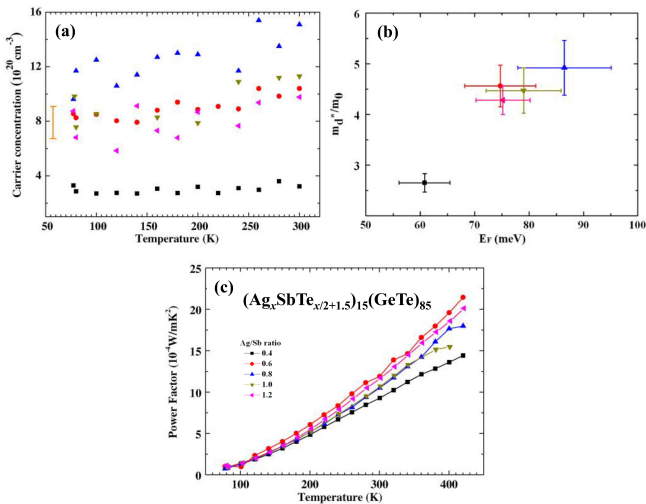


Fig. 7. Temperature dependent carrier concentration (a), Fermi energy dependent density of state effective mass (b) and temperature dependent power factor (c) for TAGS-85 with different Ag/Sb ratios.^[45] Reproduced under the terms of the CC-BY Creative Commons Attribution 3.0 License.^[45] Copyright 2014, IOP Publishing Ltd and Deutsche Physikalische Gesellschaft.

Thus, the Ag/Sb ratio of $\sim 2/3$ has been proven as the optimal composition in TAGS for the optimization of carrier concentration. Fixing the Ag/Sb atomic ratio at Ag:Sb=2:3, the effect of $(\text{Ag}_2\text{Te})_{0.4}(\text{Sb}_2\text{Te}_3)_{0.6}$ concentration on thermoelectric properties of $(\text{GeTe})_{1-x}[(\text{Ag}_2\text{Te})_{0.4}(\text{Sb}_2\text{Te}_3)_{0.6}]_x$ alloys has been investigated.^[36] The interaxial angle and m_d^* increase with increasing $(\text{Ag}_2\text{Te})_{0.4}(\text{Sb}_2\text{Te}_3)_{0.6}$ concentration,

and the interaxial angle turns into 90° as the concentration up to 25%. The increased m_d^* leads to an enhancement of Seebeck coefficient along with a reduction in Hall mobility due to the additional carrier scattering by point defects. Meanwhile, the lattice thermal conductivity lower than $\sim 0.7 \text{ W/m}\cdot\text{K}$ in the entire temperature range and the lowest value of only $0.45 \text{ W/m}\cdot\text{K}$ are achieved in TAGS-80 with Ag/Sb ratio of 2/3. Eventually, a peak zT of ~ 1.8 and an average one of ~ 1.37 in 300–800 K are realized.

5.3. Rare-earth-element doping

In order to enhance thermoelectric performance of TAGS, the rare-earth-element of Ce and Yb with the localized magnetic moment are used to substitute at Te site for introducing resonant states near the Fermi level, which enables a significant increase in Seebeck coefficient as well as electronic performance.^[38] As a result, a peak zT of 1.8 is realized in Yb-doped TAGS-85.^[40,54] In addition, substitutions of rare-earth-element Dy at Ge and Te sites have also been proven to effectively enhance thermoelectric performance in TAGS-85.^[37] Such an enhancement dominantly results from the energy filtering of the carriers by potential barriers due to the large atomic size and localized magnetic moment of Dy. Nd substitution at Sb site is found to be effective on reducing carrier concentration (Fig. 8(a)).^[60] The optimization of the carrier concentration leads to an enhanced $S^2\sigma$ of $32 \mu\text{W}\cdot\text{cm}^{-1}\cdot\text{K}^{-2}$ (Fig. 8(b)) and an extraordinary zT at 727 K in 2% Nd-doped TAGS-85 (Figs. 8(c) and 8(d)), which is comparable to that of Ce-, Yb-, and Dy-doped TAGS-85.

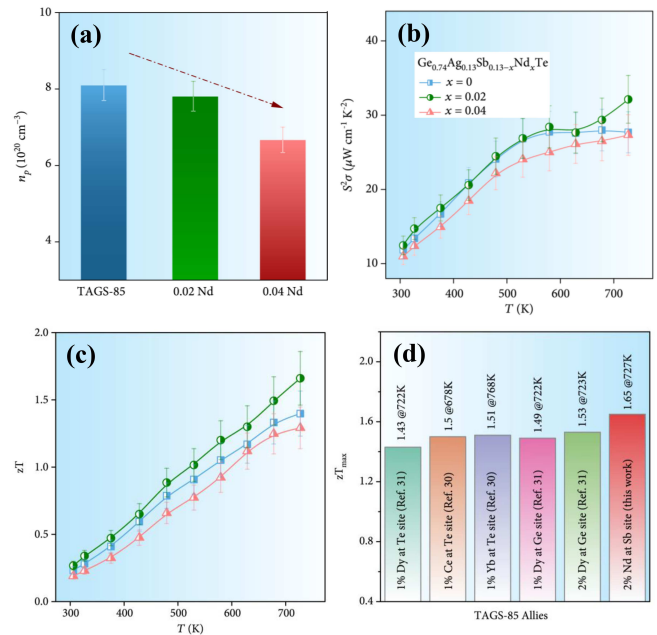


Fig. 8. Room temperature carrier concentration (a), temperature-dependent electronic performance ($S^2\sigma$) (b) and zT (c) for $\text{Ge}_{0.74}\text{Ag}_{0.13}\text{Sb}_{0.13-x}\text{Nd}_x\text{Te}$ ($x = 0, 0.02$, and 0.04). Maximal zT (d) for $\text{Ge}_{0.74}\text{Ag}_{0.13}\text{Sb}_{0.11}\text{Nd}_{0.02}\text{Te}$ with a comparison to that of the reported TAGS-85 doped with rare-earth element.^[60] Reproduced under the terms of the Creative Commons Attribution License (CC BY 4.0).^[60] Copyright 2021 Wan Yu Lyu *et al.* Exclusive Licensee Beijing Institute of Technology Press.

5.4. Lattice thermal conductivity

TAGS alloys have been revealed to possess a low lattice thermal conductivity, while it is still higher than the amorphous limit estimated by the recently developed model taking into account the periodic boundary conditions ($\kappa_L^{\min} \approx 0.13 \text{ W/m}\cdot\text{K}$).^[67,68] Therefore, a further reduction in lattice thermal conductivity is still necessary for zT -maximization.

It has been illustrated that the carrier mean free path for TAGS-85 is comparable to the lattice parameter, indicating a possibly minimal carrier mobility, the Ioffe–Regel limit.^[40] This suggests that further reduction in grain size can be beneficial for κ_L reduction while affect carrier mobility negligibly. A synthesis technique of melt spinning is applied to prepare the samples with fine grain. The lattice thermal conductivity (Fig. 9(a)) for TAGS-85 alloys with different Ag/Sb ratios is found to effectively reduced due to the strengthened phonon scattering by extra grain boundary (Fig. 9(b)).

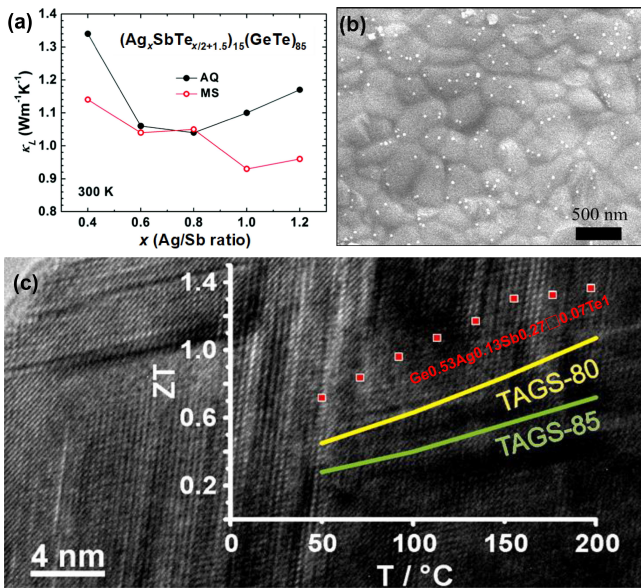


Fig. 9. Lattice thermal conductivity at room temperature for air cooled and melt-spinning TAGS-85 alloys with different Ag/Sb ratios (a), SEM image of melt-spinning ribbon of TAGS-85 alloy (b).^[40] HRTEM image and zT values of $\text{Ge}_{0.53}\text{Ag}_{0.13}\text{Sb}_{0.27}\square_{0.07}\text{Te}_1$ with a comparison to TAGS-80 and TAGS-85.^[64] (a), (b) Republished with permission of Royal Society of Chemistry, from Ref. [40]; permission conveyed through Copyright Clearance Center, Inc. (c) Reprinted with permission from Ref. [64], Copyright 2014 American Chemical Society.

In addition to the grain boundary phonon scattering, introduction of cation vacancy is also used to effectively reduce κ_L of TAGS.^[64] $\text{Ge}_{0.53}\text{Ag}_{0.13}\text{Sb}_{0.27}\square_{0.07}\text{Te}_1$ exhibits “parquet-like” multidomain nanostructures with finite intersecting vacancy layers (Fig. 9(c)), which is similar to the nanostructure observed in silver-free $(\text{GeTe})_n\text{Sb}_2\text{Te}_3$. These introduced short-range ordered cation vacancies act as phonon scattering centers, and lead to a significantly reduced lattice thermal conductivity. An extraordinary zT up to 1.3 is achieved in $\text{Ge}_{0.53}\text{Ag}_{0.13}\text{Sb}_{0.27}\square_{0.07}\text{Te}_1$ at 433 K, a temperature far below the phase transition temperature. This work opens possibility

of TAGS alloys as a candidate for low-temperature thermoelectric applications.

Inclusion of a compound with an ultralow κ_L as a second phase has been developed as an effective approach for reducing κ_L of a composite.^[69] The phase compositions of the TAGS are sensitive to the Ag/Sb ratio. Ag_8GeTe_6 precipitates could be observed in the samples with Ag/Sb ratio higher than 1.^[63] Ag_8GeTe_6 has been proven as a promising thermoelectric material with an ultralow lattice thermal conductivity of $\sim 0.26 \text{ W}\cdot\text{m}^{-1}\cdot\text{K}^{-1}$ at room temperature.^[70] Thus, a low κ_L as low as $\sim 0.2 \text{ W}\cdot\text{m}^{-1}\cdot\text{K}^{-1}$ at 700 K is realized in $(\text{GeTe})_{85}(\text{Ag}_y\text{Sb}_{2-y}\text{Te}_{3-y})_{15}$ with $y = 1.3$,^[63] which can be reasonably understood by the contribution of Ag_8GeTe_6 precipitates. The similar case has also observed in SnSe with Ag_8SnSe_6 precipitates.^[69]

6. Thermoelectric applications of TAGS alloys

The conversion efficiency for power generation primarily depends on the thermoelectric figure of merit (zT) and the temperature difference (ΔT) between the hot and cold sides of a device. Due to the outstanding thermoelectric performance, TAGS alloys have been often chosen as a p-type legs for high-efficiency thermoelectric devices, which have been used in radioisotope thermoelectric generators for aerospace missions executed by National Aeronautics and Space Administration (NASA), including the two Viking Mars landers (1976) and the Pioneers 10 and 11 (1972–1973). Moreover, the TAGS related RTGs are also used in the desert and arctic environments, such as the meteorological relay station in California and ten seismic detectors in Alaska.^[71]

In the early days, p-type TAGS alloys usually mate with n-type PbTe alloys. For single-leg or single-stage couples without segmentation, the power generation efficiency for TAGS-based devices ranges from $\sim 4\%$ to $\sim 10\%$ (Fig. 10(a)).^[57,72–74] The rare earth element (1% Yb or Ce) doped TAGS-85 alloys (identified as “e-TAGS”), developed recent years, exhibit a promising potential for thermoelectric applications.^[38,54,73,74] A three-stage device, incorporating e-TAGS materials, shows a peak device conversion efficiency as high as $\sim 20\%$ with a ΔT of 750 K.^[75]

In addition to the high zT for a high conversion efficiency, high service stability, essentially requiring thermoelectric materials with good mechanical properties, is also important for a thermoelectric device. Since the 2000s, great efforts have been devoted to optimizing the synthesis procedure for highly dense materials with excellent mechanical properties and low thermal expansion coefficients.^[59] The thermal expansion coefficient for TAGS-80 has been decreased from 18.5 ppm/K to 13.3 ppm/K by the optimization of the synthesis procedure.^[57] In addition, $(\text{GeTe})_x(\text{AgSbTe}_2)_{100-x}$ alloys with high Vickers

hardness have fabricated by a combination of gas atomization and hot-extrusion process (Fig. 10(b)).^[76]

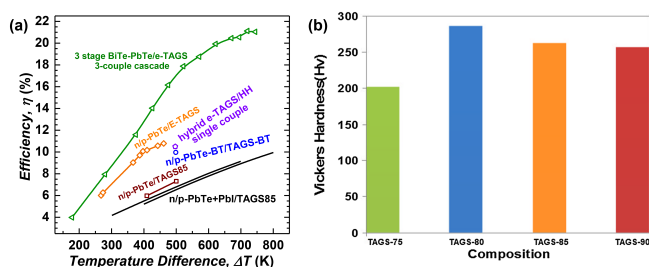


Fig. 10. Temperature difference (ΔT) dependent thermoelectric power generation efficiency (η) for TAGS based thermoelectric devices.^[57,72–75] (a), and Vickers micro-hardness values of $(\text{GeTe})_x(\text{AgSbTe}_2)_{100-x}$ ($x = 75, 80, 85$ or 90) alloys fabricated by gas-atomization and hot-extrusion processes.^[76] (b) Reprinted by permission from Springer Nature Customer Service Centre GmbH: Springer Nature, Journal of Electronic Materials,^[76] Copyright 2017, The Minerals, Metals & Materials Society.

7. Summary

In summary, TAGS- x alloys, especially those with x within 75–90, well retain the features of crystal and band structures of GeTe. The phase transition of cubic-to-rhombohedral provides a possibility of the band engineering by the variation of the interaxial angle, and thus a superior electronic performance. The inherently low lattice thermal conductivity, stemming from the strong anharmonicity and extra phonon scattering by defects, successfully ensures high zT s in both rhombohedral and cubic TAGS with optimal composition, leading these alloys to be promising p-type candidates for middle-temperature thermoelectric applications. Efforts have been made including adjusting the ratio of Ag/Sb and rare-earth-elements doping for the power factor improvement, and microstructure engineering such as grain refinement, introduction of high-concentration cation vacancies and compositing second-phase materials with low thermal conductivity for decreasing the κ_L . Through these efforts, the thermoelectric figure of merit has been significantly improved in TAGS-based alloys. Further considerations about the future directions in TAGS-based thermoelectrics are shown below.

A manipulation of the band structure by tuning the interaxial angle with a negligible effect on the carrier mobility is important, which highly relies on the discovery of efficient solvent to increase the band degeneracy. This might open new possibilities for electronic performance enhancement. Thermally, according to the model predictions, the experimentally reported lattice thermal conductivity, especially near room temperature, is still much higher than its theoretical minimum, suggesting an available room for a further reduction. This is likely realizable by manipulating the hierarchical microstructures, including the dislocations. In terms of thermoelectric devices, promoting the TAGS materials with optimized thermoelectric properties and improved mechanical strength to the

fabrication of devices will benefit the thermoelectric applications of TAGS. Particularly, development of the TAGS-based devices for thermoelectric applications near room temperature can be of great interest in the future, due to its highly competitive performance and good mechanical properties.

Acknowledgements

This work is supported by the National Natural Science Foundation of China (Grant Nos. T2125008, 92163203, and 52022068), the Innovation Program of Shanghai Municipal Education Commission, the Hefei National Laboratory for Physical Sciences at the Microscale (Grant No. KF2020007), the Shanghai Natural Science Foundation (Grant No. 19ZR1459900), Taiyuan University of Science and Technology Scientific Research Initial Funding (No. 20222002), and the project supported by State Key Laboratory of Advanced Technology for Materials Synthesis and Processing (Wuhan University of Technology, No. 2022-KF-32).

References

- [1] He R, Zhu H, Sun J, Mao J, Reith H, Chen S, Schierning G, Nielsch K and Ren Z 2017 *Materials Today Physics* **1** 24
- [2] Pei Y, Zheng L, Li W, Lin S, Chen Z, Wang Y, Xu X, Yu H, Chen Y and Ge B 2016 *Advanced Electronic Materials* **2** 1600019
- [3] Hu L, Zhu T, Liu X and Zhao X 2014 *Adv. Funct. Mater.* **24** 5211
- [4] Yu F, Meng X, Cheng J, Liu J P, Yao Y L and Li J 2019 *J. Alloys Compd.* **797** 940
- [5] Gałzka K, Xie W, Populoh S, Aguirre M H and Weidenkaff A 2020 *Rare Metals* **39** 659
- [6] Wang R F, Li S, Xue W H, Chen C, Wang Y M, Liu X J and Zhang Q 2020 *Rare Metals* **40** 40
- [7] Chen Z, Ge B, Li W, Lin S, Shen J, Chang Y, Hanus R, Snyder G J and Pei Y 2017 *Nat. Commun.* **8** 13828
- [8] Kim S I, Lee K H, Mun H A, Kim H S, Hwang S W, Roh J W, Yang D J, Shin W H, Li X S, Lee Y H, Snyder G J and Kim S W 2015 *Science* **348** 109
- [9] Vineis C, Shakouri A, Majumdar A and Kanatzidis M 2010 *Adv. Mater.* **22** 3970
- [10] Poudel B, Hao Q, Ma Y, Lan Y, Minnich A, Yu B, Yan X, Wang D, Muto A, Vashaee D, Chen X, Liu J, Dresselhaus M S, Chen G and Ren Z 2008 *Science* **320** 634
- [11] Jiang W, Ma L and Xu X 2019 *Bio-Design and Manufacturing* **2** 24
- [12] Han Q, Chen Y, Song W, Zhang M, Wang S, Ren P, Hao L, Wang A, Bai S and Yin J 2019 *Bio-Design and Manufacturing* **2** 269
- [13] Snyder G, Christensen M, Nishibori E, Caillat T and Iversen B 2004 *Nat. Mater.* **3** 458
- [14] Liu H X, Deng S P, Li D C, Shen L X and Deng S K 2017 *Chin. Phys. B* **26** 027401
- [15] Liu H, Shi X, Xu F, Zhang L, Zhang W, Chen L, Li Q, Uher C, Day T and Snyder G J 2012 *Nat. Mater.* **11** 422
- [16] Li W, Lin S, Ge B, Yang J, Zhang W and Pei Y 2016 *Advanced Science* **3** 1600196
- [17] Liu H X, Li W, Shen H W, Zhang X Y, Lin S Q and Pei Y Z 2020 *Annalen der Physik* **532** 1900561
- [18] Zhang X, Chen Z, Lin S, Zhou B, Gao B and Pei Y 2017 *ACS Energy Letters* **2** 2470
- [19] Pei Y, Shi X, LaLonde A, Wang H, Chen L and Snyder G J 2011 *Nature* **473** 66
- [20] Lin S, Li W, Chen Z, Shen J, Ge B and Pei Y 2016 *Nat. Commun.* **7** 10287
- [21] Li W, Zheng L L, Ge B H, Lin S Q, Zhang X Y, Chen Z W, Chang Y J and Pei Y Z 2017 *Adv. Mater.* **29** 1605887

- [22] Tang J, Gao B, Lin S, Li J, Chen Z, Xiong F, Li W, Chen Y and Pei Y 2018 *Adv. Funct. Mater.* **28** 1803586
- [23] Li J, Zhang X, Chen Z, Lin S, Li W, Shen J, Witting I T, Faghaninia A, Chen Y, Jain A, Chen L, Snyder G J and Pei Y 2018 *Joule* **2** 976
- [24] Tang Y, Gibbs Z M, Agapito L A, Li G, Kim H S, Nardelli M B, Curtarolo S and Snyder G J 2015 *Nat. Mater.* **14** 1223
- [25] Liu W, Tan X, Yin K, Liu H, Tang X, Shi J, Zhang Q and Uher C 2012 *Phys. Rev. Lett.* **108** 166601
- [26] Jin M, Zheng L, Sun C, Jiang L, Meng X, Chen Q and Li W 2021 *Chem. Eng. J.* **420** 130530
- [27] Pei Y, LaLonde A D, Wang H and Snyder G J 2012 *Energy & Environmental Science* **5** 7963
- [28] Wang H, LaLonde A D, Pei Y and Snyder G J 2013 *Adv. Funct. Mater.* **23** 1586
- [29] You L, Zhang J, Pan S, Jiang Y, Wang K, Yang J, Pei Y, Zhu Q, Agne M T, Snyder G J, Ren Z, Zhang W and Luo J 2019 *Energy & Environmental Science* **12** 3089
- [30] Jood P, Ohta M, Yamamoto A and Kanatzidis M G 2018 *Joule* **2** 1339
- [31] Li S, Xin J, Basit A, Long Q, Li S, Jiang Q, Luo Y and Yang J 2020 *Adv. Sci. (Weinh)* **7** 1903493
- [32] Guo F, Cui B, Li C, Wang Y, Cao J, Zhang X, Ren Z, Cai W and Sui J 2021 *Adv. Funct. Mater.* **31** 2101554
- [33] Xing T, Song Q, Qiu P, Zhang Q, Gu M, Xia X, Liao J, Shi X and Chen L 2021 *Energy & Environmental Science* **14** 995
- [34] Xing T, Zhu C, Song Q, Huang H, Xiao J, Ren D, Shi M, Qiu P, Shi X, Xu F and Chen L 2021 *Adv. Mater.* **33** 2008773
- [35] Li J, Chen Z W, Zhang X Y, Sun Y X, Yang J and Pei Y Z 2017 *NPG Asia Materials* **9** e353
- [36] Liu H X, Zhang X Y, Bu Z L, Li W and Pei Y Z 2022 *Rare Metals* **41** 921
- [37] Levin E M, Bud'ko S L and Schmidt-Rohr K 2012 *Adv. Funct. Mater.* **22** 2766
- [38] Levin E M, Cook B A, Harringa J L, Bud'ko S L, Venkatasubramanian R and Schmidt-Rohr K 2011 *Adv. Funct. Mater.* **21** 441
- [39] Rodenkirchen C, Cagnoni M, Jakobs S, Cheng Y D, Keutgen J, Yu Y, Wuttig M and Cojocar-Miredin O 2020 *Adv. Funct. Mater.* **30** 1910039
- [40] Zhu T, Gao H, Chen Y and Zhao X 2014 *J. Mater. Chem. A* **2** 3251
- [41] Hong M, Chen Z G, Yang L, Liao Z M, Zou Y C, Chen Y H, Matsumura S and Zou J 2018 *Advanced Energy Materials* **8** 1702333
- [42] Chattopadhyay T, Bouchler J X and Vonscherner H G 1987 *J. Phys. C: Solid State Phys.* **20** 1431
- [43] Baleva M I and Plachkova S K 1983 *J. Phys. C: Solid State Phys.* **16** 791
- [44] Plachkova S K 1984 *Physica Status Solidi (a)* **83** 349
- [45] Chen Y, Jaworski C M, Gao Y B, Wang H, Zhu T J, Snyder G J, Heremans J P and Zhao X B 2014 *New J. Phys.* **16** 013057
- [46] Cook B A, Kramer M J, Wei X, Harringa J L and Levin E M 2007 *J. Appl. Phys.* **101** 053715
- [47] Hsu K F, Loo S, Guo F, Chen W, Dyck J S, Uher C, Hogan T, Polychroniadis E K and Kanatzidis M G 2004 *Science* **303** 818
- [48] Cook B A, Wei X, Harringa J L and Kramer M J 2007 *Journal of Materials Science* **42** 7643
- [49] Yang S H, Zhu T J, Sun T, He J, Zhang S N and Zhao X B 2008 *Nanotechnology* **19** 245707
- [50] Kumar A, Vermeulen P A, Kooi B J, Rao J, van Eijck L, Schwarzmüller S, Oeckler O and Blake G R 2017 *Inorg. Chem.* **56** 15091
- [51] Davidow J and Gelbstein Y 2012 *Journal of Electronic Materials* **42** 1542
- [52] Thompson A, Sharp J, Rawn C J and Chackoumakos B C 2007 *Mater. Res. Soc. Symp. P* **1044** 1044-U03-09
- [53] Kumar A, Vermeulen P A, Kooi B J, Rao J, Schwarzmüller S, Oeckler O and Blake G R 2018 *RSC Advances* **8** 42322
- [54] Cook B A, Harringa J L, Besser M and Venkatasubramanian R 2011 *Mater. Res. Soc.* **1325** 703
- [55] Kim B S, Kim I H, Lee J K, Min B K, Oh M W, Park S D, Lee H W and Kim M H 2010 *Electronic Materials Letters* **6** 181
- [56] Dong Y, Malik A S and DiSalvo F J 2010 *Journal of Electronic Materials* **40** 17
- [57] Skrabek E A and Trimmer D S 1972 *US Patent* **3** 945 [1976-3-23]
- [58] Zybala R 2020 *Synthetic Metals* **270** 116606
- [59] Salvador J R, Yang J, Shi X, Wang H and Wereszczak A A 2009 *J. Solid State Chem.* **182** 2088
- [60] Lyu W Y, Hong M, Liu W D, Li M, Sun Q, Xu S D, Zou J and Chen Z G 2021 *Energy Material Advances* **2021** 2414286
- [61] Christakudis G C, Plachkova S K, Shelimova L E and Avilov E S 1991 *Physica Status Solidi (a)* **128** 465
- [62] Chen Y, Zhu T J, Yang S H, Zhang S N, Miao W and Zhao X B 2010 *Journal of Electronic Materials* **39** 1719
- [63] Jin J, Zhu T J, Liu X H and Zhao X B 2013 *Journal of Materials Science and Engineering* **31** 204 (in Chinese)
- [64] Schroder T, Rosenthal T, Giesbrecht N, Nentwig M, Maier S, Wang H, Snyder G J and Oeckler O 2014 *Inorg. Chem.* **53** 7722
- [65] Yang S H, Zhu T J, Yu C, Shen J J, Yin Z Z and Zhao X B 2011 *Journal of Electronic Materials* **40** 1244
- [66] Schröder T, Rosenthal T, Giesbrecht N, Maier S, Scheidt E W, Scherer W, Snyder G J, Schnick W and Oeckler O 2014 *J. Mater. Chem. A* **2** 6384
- [67] Chen Z, Zhang X, Lin S, Chen L and Pei Y 2018 *National Science Review* **5** 888
- [68] Snyder G J, T. Agne M and Gurunathan R 2018 *National Science Review* **6** 380
- [69] Luo Y, Cai S, Hua X, Chen H, Liang Q, Du C, Zheng Y, Shen J, Xu J, Wolverson C, Dravid V P, Yan Q and Kanatzidis M G 2018 *Advanced Energy Materials* **9** 1803072
- [70] Zhu T J, Zhang S N, Yang S H and Zhao X B 2010 *Physica Status Solidi (RRL) - Rapid Research Letters* **4** 317
- [71] Skrabek E A and Trimmer D S 1995 *Properties of the general TAGS system. In CRC handbook of thermoelectrics* (Boca Raton, FL: CRC Press) pp. 267–275
- [72] Singh A, Bhattacharya S, Thinakaran C, Aswal D K, Gupta S K, Yakhmi J V and Bhanumurthy K 2009 *J. Phys. D: Appl. Phys.* **42** 015502
- [73] Thomas P, Cook B, Stokes D, Krueger G and Venkatasubramanian R 2012 *Proc. of SPIE* **8377** 83770H-1
- [74] Bulman G and Cook B 2014 *Proc. SPIE* **9115** 911507-1
- [75] Cook B A, Chan T E, Dezi G, Thomas P, Koch C C, Poon J, Tritt T and Venkatasubramanian R 2015 *Journal of Electronic Materials* **44** 1936
- [76] Kim H S, Dharmiah P and Hong S J 2017 *Journal of Electronic Materials* **47** 3119